Preparation of efficient and recoverable organosulfonic acid functionalized alkyl-bridged organosilica nanotubes for esterification and transesterification

Xianghuan Zhang [a], Fang Su [a], Daiyu Song [a], Sai An [a], Bo Lu [a], Yihang Guo [a,b,*]

[a] School of Chemistry, Northeast Normal University, Changchun 130024, P.R. China
[b] School of Environment, Northeast Normal University, Changchun 130117, P.R. China

ARTICLE INFO

ABSTRACT

A series of arenesulfonic or propylsulfonic acid functionalized ethane- or benzene-bridged organosilica nanotubes hybrid catalysts, $Si(Ph/Et)Si-Ar/Pr-SO_3H$ NTs, was demonstrated for the first time by a single step nonionic surfactant-templated sol–gel co-condensation approach. The pore morphologies, textual and acidic properties of as-prepared hybrid catalysts were characterized by TEM observations, nitrogen gas porosimetry measurements and acid–base titration, while the structural integrity of the incorporated organosulfonic acid groups and silica/carbon framework in the hybrid catalysts were studied by ^{13}C CP-MAS NMR and ^{29}Si MAS NMR. As the novel solid acid catalysts, the catalytic activity and stability of the $Si(Ph/Et)Si-Ar/Pr-SO_3H$ NTs were evaluated by esterification of palmitic acid and transesterification of yellow horn seed oil with methanol under refluxing temperature ($65\,^\circ C$) and atmospheric pressure. Based on the physicochemical properties and catalytic testing results, the excellent heterogeneous acid catalytic behaviors of as-prepared tubular hybrid catalysts were revealed in terms of their considerably high Brønsted acid-site density and acid strength, unique textural properties, interesting morphology as well as hydrophobic surface.

© 2014 Elsevier B.V. All rights reserved.

1. Introduction

The use of solid acids for "*second generation*" biodiesel production from inedible oily feedstocks is an emerging research field. Recent studies have proved the technical feasibility and the environmental and economical benefits of heterogeneous acid-catalyzed simultaneous esterification and transesterification for biodiesel production [1–4]. Numerous solid acids such as sulfated metal oxides [5–8], H-form zeolites [9], sulfonic ion-exchange resins [10], sulfonic acid modified mesostructured silica materials [11], sulfonated carbon-based catalysts [12], heteropolyacids [13], SiO_2-, ZrO_2- or Ta_2O_5-supported heteropolyacids [14–18] and acidic ionic liquids [19] have been extensively studied for this topic. Although these solid acids show acceptable reactivity towards esterification of long chain free fatty acids (FFAs), their reactivity to the transesterification of viscous and bulky triglycerides (TGs)-containing oily feedstocks is generally unsatisfactory. Therefore, most of solid acid-catalyzed transesterification reactions proceed under stringent conditions including higher temperature, higher pressure, an excess of alcohol as well as longer reaction time, which are not favorable for industrial applications. Moreover, solid acid catalysts often suffer from problems of deactivation, poisoning and acid site leaching in the reaction medium. Thereby, design of efficient, robust and catalytically stable solid acid catalysts that can improve the overall efficiency of biodiesel production dramatically is still an important challenge.

Arenesulfonic or alkylsulfonic acid functionalized inorganic mesoporous silica or periodic mesoporous organosilica (PMO) materials are one of the most robust solid acid catalysts owing to their high Brønsted acid strength and plentiful number of acid sites. *In situ* incorporation of organosulfonic acid groups throughout the silica framework is a better method to construct the organosulfonic acid functionalized silica materials, and the preparation process includes the co-hydrolysis and -condensation of a tetralkoxysilane or a organosilane with 3-mercaptopropyltrialkyloxysilane (MPTMS) followed by oxidation of the thiol groups with H_2O_2. Additionally, 2-(4-chlorosulfonylphenyl)ethyl trimethoxysilane (CSPTMS) is also an useful precursor for replacement of MPTMS, which yields arenesulfonic acid groups just by hydrolysis and condensation under the acidic preparation conditions [11].

* Corresponding author. Tel./fax: +86 431 85098705.
E-mail address: guoyh@nenu.edu.cn (Y. Guo).

In comparison to post-modification approach, this one step preparation strategy can lead to organosulfonic acid functionalized silica materials with tunable loading of sulfonic acid groups, excellent textural properties and homogeneous distribution of the active phases throughout the structure of the materials; meanwhile, the hydrolytic sol–gel process can strengthen the interaction between the acid sites and silica support, and thereby enhancing the stability of the hybrid catalysts owing to the reduced leaching of the active phase [20,21]. These sulfonic acid functionalized silica materials have been applied in a wide range of organic reactions including alkylation and acylation of hydrocarbons, the hydration of alkenes and the polymerization of THF [22,23], and they are also of interest for biomass conversion-related reactions such as esterification, transesterification, hydrolysis and dehydration [24–28]. However, for the sulfonic acid functionalized silica-catalyzed biomass conversion, bulky reactants and products lead to the process serious mass-transport limitation problems and thereby insufficient accessibility of the catalytic sites, which significantly limits their catalytic activity. Meanwhile, the catalysts often suffer from severe deactivation due to accumulation of organic or carbonaceous materials on the surface; additionally, leaching of sulfonic acid groups into the reaction media may also reduce the catalytic activity after several times' cycles.

To solve the above problems, in this work, a series of arenesulfonic or propylsulfonic acid functionalized ethane- or benzene-bridged organosilica nanotubes were demonstrated for the first time by a single step nonionic surfactant-templated sol–gel co-condensation approach, and the procedure includes co-hydrolysis and -condensation of bissilylated organic precursor (*e.g.* 1,2-bis-(trimethoxysilyl)ethane or 1,4-bis-(triethoxysilyl)benzene) and CSPTMS (MPTMS) in the presence of P123 under acidic conditions. Motivation for development of this kind of organosulfonic acid functionalized silica/carbon nanotubes hybrid catalysts is to improve the acid catalytic activity of organosulfonic acid-based materials in esterification and transesterification further. It is generally accepted that the catalytic activity is closely related to the morphological and textural properties of the catalyst in addition to its structure and composition [29]. One-dimensional tubular catalysts possess large fraction of voids in the interior, allowing most of the active sites being confined inside the tubes except for external surface. Moreover, the nanotubular catalysts generally possess hierarchical pore systems, originating from hollow nanotube channels and void space between tubular nanoparticles. This property leads to the active sites are highly accessible to most common reagents and favorable to efficient reactant diffusion during the catalytic reactions. Meanwhile, they have large surface areas with flexible structure that are contributed from both outer and interior surface, which can provide more active sites to promote the reactions. Successful construction of inorganic nanotube catalysts (e.g. TiO_2 nanotube photocatalyst [30]) or functional group modified inorganic nanotubes (e.g. salen-metal complex functionalized carbon nanotube [31]) have emerged recreantly, however, preparation of organosilica nanotubes or functional groups modified organosilica nanotubes with bridging alkyl groups and/or active sites within the framework have seldom been reported up till now. By the combination of the advantages such as strong Brønsted acidity, high mechanical and hydrothermal stability, tunable surface hydrophobicity/hydrophilicity, excellent textural properties and interesting morphological characteristics, as-designed organosulfonic acid functionalized alkyl-bridged organosilica nanotubes are expected as the promising solid acid catalyst candidates for biodiesel production [32–35]. Additionally, because organosulfonic groups were incorporated into the organosilica wall (Schemes 1 and 2), agglomeration or leaching of the functional groups is expected to be avoided, leading to the increased catalytic stability of these kinds of the catalysts beside the activity [20].

To evaluate the heterogeneous acid catalytic performance of as-prepared organosulfonic acid functionalized alkyl-bridged organosilica nanotubes, esterification of palmitic acid (one of typical FFAs existed in inedible oily feedstocks) and transesterification of yellow horn (or *Xanthoceras sorbifolia* Bunge, a kind of inedible plant) seed oil with methanol under refluxing temperature (65 °C) and atmospheric pressure are selected as the model reactions. The tested hybrid catalysts include arenesulfonic acid functionalized ethane-bridged organosilica nanotubes (Si(Et)Si-Ar-SO_3H NTs), arenesulfonic acid functionalized benzene-bridged organosilica nanotubes (Si(Ph)Si-Ar-SO_3H NTs) and propylsulfonic acid functionalized ethane-bridged organosilica nanotubes (Si(Et)Si-Pr-SO_3H NTs). For comparision, the prepared arenesulfonic acid functionalized SBA-15 inorganic silica with two-dimensional hexagonal $p6\,mm$ mesostructure (SBA-15-Ar-SO_3H), three-dimensional worm-like arenesulfonic acid functionalized benzene-bridged organosilica obtained in the absence of P123 (P123 free Si(Ph)Si-Ar-SO_3H) and commercially available sulfonic ion-exchange resin (Amberlyst-15) are also tested under the same conditions. Based on the catalytic testing results, the influence of Brønsted acid strength and acid-site density, morphological and textural properties as well as surface hydrophobicity on the acid catalytic activity of as-prepared organosulfonic acid based hybrid catalysts is discussed. Finally, the recyclability of the hybrid catalysts is tested through three consecutive catalytic runs.

2. Experimental

2.1. Materials

Tetraethylorthosilicate (TEOS, 98%), 3-mercaptopropyltriethoxysilane (MPTMS, 95%), 1,2-bis(trimethoxysilyl)ethane (BTMSE, 97%), 1,4-bis-(triethoxysilyl)benzene (BTESB, 96%) and Pluronic P123 ($EO_{20}PO_{70}EO_{20}$, where $EO = -CH_2CH_2O-$, $PO = -CH_2(CH_3)CHO-$, $M_W = 5800$) were purchased from Sigma–Aldrich and used without further purification. 2-(4-chlorosulfonylphenyl)ethyl trimethoxysilane (CSPTMS, 50% in dichloromethane) was obtained from Gelest Inc. Commercially available Amberlyst-15 (Alfa Aesar) was used as a reference catalyst. Palmitic acid (99%) was obtained from Tianjin Guangfu fine chemical research institute (China). Yellow horn seed oil is commercially available. All other chemicals were analytical grade, and they were purchased from Beijing Fine Chemical Co. (China).

2.2. Preparation of organosulfonic acid functionalized alkyl-bridged organosilica nanotubes

2.2.1. Arenesulfonic acid functionalized ethane-bridged organosilica nanotubes (Si(Et)Si-Ar-SO_3H NTs)

Direct co-hydrolysis followed by co-condensation of BTMSE and CSPTMS in the presence of P123 was applied to prepare Si(Et)Si-Ar-SO_3H NTs. Typically, P123 (4 g) was dissolved in HCl (1.9 mol L^{-1}, 125 g) at room temperature under stirring. The clear P123 solution was heated to 40 °C, and then BTMSE was added. A BTMSE prehydrolysis time of 45 min was used prior to the addition of CSPTMS to the above mixture. The resultant white suspension with molar composition of (0.0195 − 0.0164) BTMSE: (0.0021 − 0.0082) CSPTMS: 0.24 HCl: 6.67 H_2O was stirred at 40 °C for 24 h. Subsequently, the suspension was transferred to an autoclave and heated at 100 °C with a heating rate of 2 °C min^{-1} for additional 24 h. The solid product was recovered by filtration and air-dried at 60 °C overnight. Finally, boiling ethanol washing for 12 h was applied to remove P123 from the product, and the procedure was repeated for three times. The product obtained after air-dried at 60 °C for 24 h is
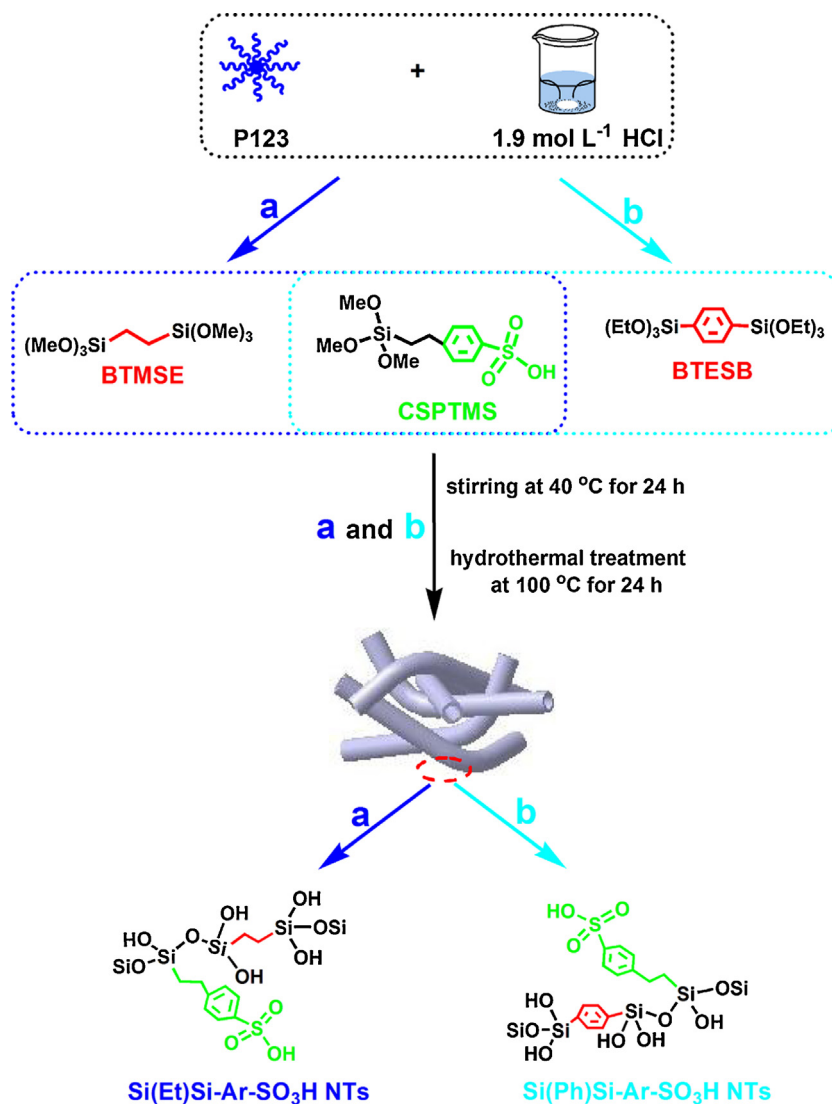
Scheme 1. Illustration of one-step preparation of arenesulfonic acid functionalized ethane- (a) or benzene-bridged (b) organosilica nanotubes.

denoted as Si(Et)Si-Ar-SO$_3$H–x NTs, where x represents molar percentage of −SO$_3$H group in CSPTMS with respect to total silicon in the initial gel mixture, i.e. x (mol %) = CSPTMS/(2BTMSE + CSPTMS).

For comparison, ethane-bridged organosilica nanotubes (Si(Et)Si NTs) was prepared by the aforementioned route in the absence of CSPTMS.

2.2.2. Arenesulfonic acid functionalized benzene-bridged organosilica nanotubes (Si(Ph)Si-Ar-SO$_3$H NTs)

Si(Ph)Si-Ar-SO$_3$H NTs with x (mol %) = 10 was prepared by the aforementioned route but replacement of BTMSE for BTESB, and the starting molar composition of the reactants is 0.0185 BTESB: 0.0041 CSPTMS: 0.24 HCl: 6.67 H$_2$O.

For comparison, benzene-bridged organosilica nanotubes (Si(Ph)Si NTs) or P123 free Si(Ph)Si-Ar-SO$_3$H particles was prepared by the aforementioned route in the absence of CSPTMS or P123.

2.2.3. Propylsulfonic acid functionalized ethane-bridged organosilica nanotubes (Si(Et)Si-Pr-SO$_3$H NTs)

Si(Et)Si-Pr-SO$_3$H NTs with x (mol%) = 10 was prepared by the aforementioned route but using MPTMS (in the presence of 30 wt% H$_2$O$_2$) instead of CSPTMS as sulfonic group precursor, and the

starting molar composition of the reactants was 0.0185 BTMSE: 0.0041 MPTMS: 0.24 HCl: 6.67 H$_2$O: 0.0369 H$_2$O$_2$.

2.2.4. Ordered mesoporous arenesulfonic acid functionalized SBA-15 silica materials (SBA-15-Ar-SO$_3$H)

SBA-15-Ar-SO$_3$H with x (mol %) = 10 was prepared by the procedure similar to that of the aforementioned Si(Et)Si-Ar-SO$_3$H–10 NTs materials but using TEOS instead of bissilylated organic precursor BTMSE as the silica precursor, and the starting molar composition of the reactants was 0.0369 TEOS: 0.0041 CSPTMS: 0.24 HCl: 6.67 H$_2$O.

2.3. Characterization of the catalysts

Nitrogen gas porosimetry measurements were performed on a Micromeritics ASAP 2020M surface area and porosity analyzer after the samples were outgassed under vacuum at 363 K for 1 h and 373 K for another 12 h. TEM observations were performed on a JEM-2100F high resolution transmission electron microscope at an accelerating voltage of 200 kV. ^{13}C cross polarization-magic angle spinning (CP-MAS) NMR and ^{29}Si MAS NMR spectra were recorded on a Bruker AVANCE III 400 WB spectrometer equipped
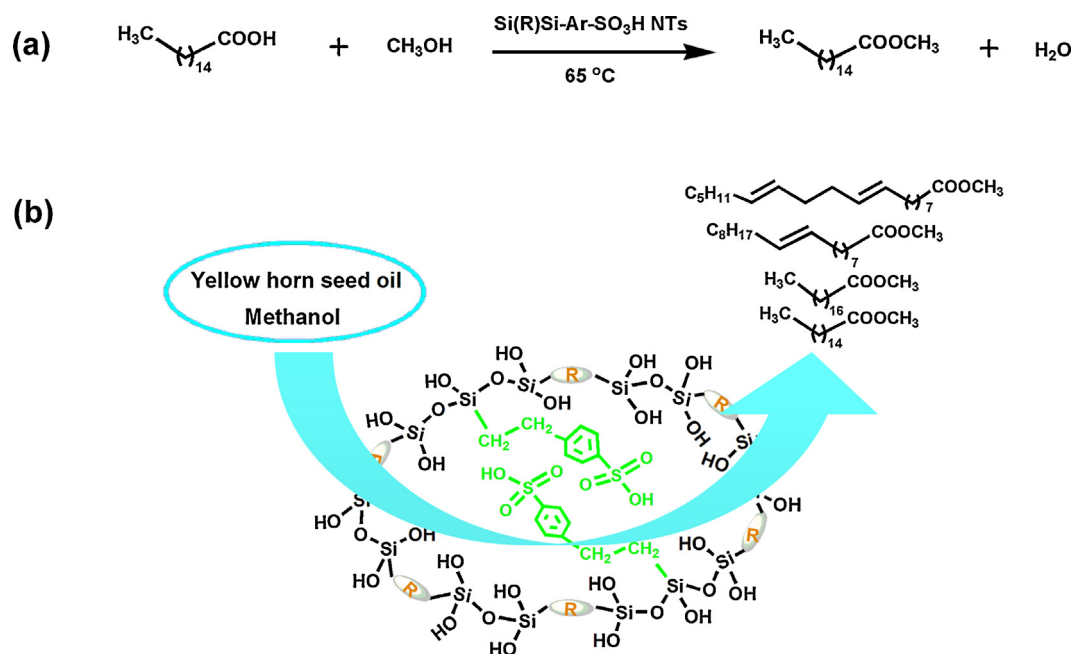
Scheme 2. Schematic presentation of wall structure of arenesulfonic acid functionalized alkyl-bridged organosilica nanotubes (Si(R)Si-Ar-SO$_3$H, R = Et/Ph) and the process of palmitic acid esterification (a) and yellow horn seed oil transesterification (b) over the Si(R)Si-Ar-SO$_3$H nanohybrid catalysts.

with a 4 mm standard bore CP MAS probe head. The dried and finely powdered samples were packed in the ZrO$_2$ rotor closed with Ke–F cap which were spun at 12 KHz rate. Chemical shifts for ^{13}C CP-MAS NMR and ^{29}Si MAS NMR spectra were referenced to the signal of C$_{10}$H$_{16}$ standard (δCH$_2$ = 38.5) and 3-(trimethylsilyl)-1-propanesulfonic acid sodium salt standard (δ = 0.0), respectively. Sulfur content or loading of —SO$_3$H group in as-prepared hybrid materials was determined by an ICAP6300-Thermoscientific ICP-OES. Before determination, the samples were dissolved by 2 mol L^{-1} NaOH and then diluted with deioned water to suitable volumes. Thermogravimetric analysis (TGA) was performed on a Shimadzu TG instrument at a heating rate of 10 °C min^{-1} in air.

The quantification of the Brønsted acidity of as-prepared organosulfonic acid modified silica materials was carried out through ion exchange with 2 mol L^{-1} of NaCl solution (10 g), leaving it in contact with the sample powder (0.0500 g) at 30 °C for 24 h. The evaluation of H$^+$ concentration was then performed by titration with 0.0095 mol L^{-1} of NaOH standard solution. The number of H$^+$ microequivalents released per gram of catalyst was then calculated.

2.4. Catalytic tests

The catalysts were dried for 2 h at 120 °C in a vacuum before the catalytic tests. Esterification of palmitic acid with methanol was performed at 65 °C, palmitic acid to methanol molar ratio of 1:5 and 2 wt% (with respect to the amount of reactants) catalyst. Transesterification of yellow horn seed oil with methanol was performed at 65 °C, 1.1 mmol yellow horn seed oil, 3.8 mL methanol and 5 wt% (with respect to the amount of reactants) catalyst.

At periodical intervals, 0.1 mL of the reaction mixture was withdrawn and then diluted with acetone to 5 mL. The diluted suspension was centrifuged, and the clear solution was analyzed by a Shimadzu 2014C gas chromatograph (GC) to obtain the concentrations of the produced FAMEs. The GC was equipped with a HP-INNOWAX capillary column (film thickness, 0.5 μm; i.d., 0.32 mm; length, 30 m) and flame ionization detector. The operation temperature was 230 °C, flow rate of nitrogen gas was 1.0 mL min^{-1}, and ethyl laurate was applied as an internal standard.

The catalytic activity of the catalysts was evaluated quantitatively by the yields of the FAMEs (Y, %). For the esterification of palmitic acid with methanol, Y was calculated as follows: Y (%) = (M_D/M_T) × 100, where M_D and M_T are the number of moles of methyl palmitate (MP) produced and expected, respectively. For the transesterification of yellow horn seed oil with methanol, Y was calculated as follows: Y (%) = (M_D/M_T) × 100, where M_D and M_T are the number of moles of FAMEs produced and expected, respectively. Through a mass spectrometry coupled with gas chromatography (HP6890GC-5973MSD) analysis, four main products including methyl palmitate (MP), methyl stearate (MS), methyl oleate (MO) and methyl lioleate (ML) together with a small quantity of methyl eicosenoate (ME) and methyl docosenate (MD) were found in the above catalytic system. The GC-MS was equipped with HP-5MS capillary column (30 m length, 0.2 mm i.d., 0.25 μm film thickness) and helium as the carrier gas at 1 mL min^{-1}. The temperature program was as follows: 150 °C for 2 min, 5 °C/min up to 250 °C, hold time of 10 min. The GC injector and MS ion source temperatures were 250 °C and 230 °C, respectively. The MS detector was operated in the EI mode at 70 eV with a scanning range of m/z 20–500. The transesterification activity of the tested catalysts was evaluated by the yields of the aforementioned four main products.

In addition, FFA existed in yellow horn seed oil was identified by an Agilent 1200 series liquid chromatograph system coupled with Bruker micrOTOF II mass spectrometry (LC-MS) (source type, ESI). Before analysis, FFA was extracted from yellow horn seed oil based on the following procedures. Yellow horn seed oil (1 mL) was added in a sodium hydroxide solution (40 mL, 6 mol L^{-1}) at 90 °C for 30 min under stirring. After the solution was cooled, 20 mL water was added. Then, the acidity of the mixture was adjusted to pH < 1 by HCl (6 mol L^{-1}) so that FFA was condensed. Finally, the condensed FFA was recovered by filtration and vacuum-dried at 40 °C overnight. The dried FFA was dissolved with acetonitrile for LC-MS analysis. The result indicated FFA existed in yellow horn seed oil was palmitic acid.

In order to evaluate the external mass-transport limitation in current systems, the influence of the stirring rate on the catalytic activity of the Si(Ph)Si-Ar-SO$_3$H NTs is studied by selecting Si(Ph)Si-Ar-SO$_3$H–10 NTs as the representative catalyst and PA esterification

as the model reaction. It shows that the catalytic activity of the Si(Ph)Si-Ar–SO$_3$H–10 NTs is hardly affected by changing the stirring rate from 300, 600, 900 to 1200 rpm, implying that the Si(Ph)Si-Ar-SO$_3$H–10 NTs-catalyzed PA esterification reaction is free from the external mass transfer limitations. Therefore, for all catalytic tests, the stirring rate is adjusted to ca. 900 rpm roughly, which can ensure complete mixing of the catalyst powder and the reactants.

3. Results and discussion

3.1. Preparation and characterization of organosulfonic acid functionalized alkyl-bridged organosilica nanotubes

Organosulfonic acid functionalized alkyl-bridged organosilica nanotubes were prepared by a single step sol–gel co-condensation approach, and the procedure included co-hydrolysis and -condensation of bissilylated organic precursor (e.g. BTMSE or BTESB) and −SO$_3$H group precursor (e.g. CSPTMS or MPTMS) by using triblock copolymer surfactant P123 as the template in acidic solution. During construction of arenesulfonic acid functionalized ethane- or benzene-bridged organosilica nanotubes, Si(Et)Si-Ar-SO$_3$H NTs or Si(Ph)Si-Ar-SO$_3$H NTs, arenesulfonic acid groups were directly introduced into the silica/carbon framework by using CSPTMS precursor (Scheme 1). As for the propylsulfonic acid functionalized ethane-bridged organosilica nanotubes, Si(Et)Si-Pr-SO$_3$H NTs, −SH groups from MPTMS were firstly incorporated into the silica/carbon framework, and then propylsulfonic acid functionalized ethane-bridged organosilica nanotubes were fabricated after H$_2$O$_2$ oxidation. It is supposed that the latter two step-route of incorporation of sulfonic acid groups may lead to some −SO$_3$H group leakage [36].

3.1.1. Pore morphologies and textual properties

The tubular nanostructures of as-prepared Si(Et/Ph)Si-Ar-SO$_3$H NTs and Si(Et)Si-Pr-SO$_3$H NTs were revealed by TEM observations, and for comparison, TEM images of −SO$_3$H-free ethane- or benzene-bridged organosilica nanotubes Si(Et/Ph)Si NTs, arenesulfonic acid functionalized SBA-15 silica SBA-15-Ar-SO$_3$H and P123 free Si(Ph)Si-Ar-SO$_3$H were also provided (Fig. 1). From Fig. 1a it is clearly seen the hollow and tubular nanostructures of Si(Et)Si NTs with several tubes twisting together. As for the Si(Et)Si-Ar-SO$_3$H NTs, the similar morphology to that of Si(Et)Si NTs can also been found, and aggregation among the tubualr nanoparticles become obvious with increasing arenesulfonic acid group molar percentage from 5 to 20 mol% (Fig. 1b–e). Fig. 1f–h is the TEM images of Si(Et)Si-Pr-SO$_3$H–10 NTs, Si(Ph)Si NTs and Si(Ph)Si-Ar-SO$_3$H–10 NTs, and they also exhibit unambiguous tube-shaped morphology. By comparison of TEM image of Si(Et)Si-Ar-SO$_3$H–10 NTs (Fig. 1c) with Si(Ph)Si-Ar-SO$_3$H–10 NTs (Fig. 1 h) it is found that the tubular nanostructure of arenesulfonic acid functionalized benzene-bridged organosilica nanotubes is perfect to arenesulfonic acid functionalized ethane-bridged organosilica nanotubes, and the inner diameter of Si(Ph)Si-Ar-SO$_3$H–10 NTs (ca. 9 nm) is larger than that of the Si(Et)Si-Ar-SO$_3$H–10 NTs (ca. 7 nm). In the case of SBA-15-Ar-SO$_3$H–10, it displays long-range hexagonal arrangement of parallel pore channels rather than tubular structure (Fig. 1i), while P123 free Si(Ph)Si-Ar-SO$_3$H–10 exhibits 3D interconnected structure with obvious particle aggregation (Fig. 1j).

Combination of the above TEM observations and the hybrid catalysts preparation routes, it is inferred that both bissilylated organic precursor and P123 template are indispensible for the construction of tube-like organosulfonic acid functionalized silica materials. Additionally, in situ incorporation of organosulfonic acid groups with wide range loading has little influence on their morphological properties, regardless of the types of −SO$_3$H group precursors.

On the one hand, in an acidic solution, the triblock copolymer surfactant P123 is known to self-assemble to rodlike micelles. On the other hand, bridging organosilanes (e.g. BTMSE or BTESB) has some different characteristics from inorganic silane precursor (e.g. TEOS and TMOS) such as a faster hydrolysis and condensation rate, surface hydrophobicity and rigidity, which is beneficial for the formation of the individual nanoparticles instead of consolidated porous structures during self-assembly process [34,37]. The interaction between P123 and the hydrolyzed organosilane precursor ensure to construct tubular Si(Ph/Et)Si-Ar/Pr-SO$_3$H nanohybrids. However, in the absence of P123, neither tubular nor ordered mesoporous structure can be fabricated, implying the important structure directing function of P123.

The textual properties of various organosulfonic acid functionalized silica or organosilica materials are studied by nitrogen gas porosimetry measurements. Fig. 2a presents the nitrogen gas adsorption–desorption isotherms of arenesulfonic acid functionalized ethane-bridged organosilica nanotubes with functional group loading of 0, 5, 10, 15, and 20 mol%. These five tested nanohybrids exhibit type IV isotherms, indicating the mesoporosity of them. For the Si(Et)Si NTs, Si(Et)Si-Ar-SO$_3$H–5 NTs, Si(Et)Si-Ar-SO$_3$H–10 NTs and Si(Et)Si-Ar-SO$_3$H–15 NTs, their nitrogen gas sorption isotherms feature two capillary condensation steps at a relative pressure of 0.50–0.70 and 0.90–0.99 (close to the saturation vapor pressure), respectively. As for the Si(Et)Si-Ar-SO$_3$H–20 NTs, only one capillary condensation step at a relative pressure of 0.50–0.80 is found. The result indicates that at arenesulfonic acid group loading lower than or equal to 15 mol%, Si(Et)Si NTs and Si(Et)Si-Ar-SO$_3$H NTs nanohybrids have bimodal pore structure, contributing from both the hollow nanotube channel and void space between the loosely packed nanotubes particles. Similar results have separately been reported by Yang's and Kruk's group [34,37]. However, when a large amount of arenesulfonic acid groups are incorporated within the wall of silica/carbon framework (e.g. arenesulfonic acid group loading reaches to 20 mol%), the hollow nanotube channel and void space are blocked severely, leading to the nanohybrid with one type of mesopore centering at 3.8 nm. The above results are consistent with BJH pore-size distribution curves displayed in Fig. 2b as well as the calculated textual parameters summarized in Table 1. From Fig. 2b it is found that the smaller (primary) pore of Si(Et)Si NTs or Si(Et)Si-Ar-SO$_3$H NTs is well-distributed featuring narrower curve, and this type of pore corresponds to uniform nanotube channel of the hybrid materials. As for the larger (secondary) pore in Fig. 2b, it is uneven-distributed featuring wider curve. This type of pore comes from void space between the loosely packed nanotubes particles.

Based on the results summarized in Table 1 it is found that pure ethane-bridged organosilica nanotubes possess the largest BET surface area (838 m^2 g^{-1}) and pore diameter (5.1 and 31.7 nm) as well as the highest pore volume (1.73 cm^3 g^{-1}). After introduction of arenesulfonic acid group at a lower loading (e.g. 5 or 10 mol%) within the wall of silica/carbon framework, the formed Si(Et)Si-Ar-SO$_3$H NTs nanohybrids have textural characteristic very similar to those of pure Si(Et)Si NTs. As for the Si(Et)Si-Ar-SO$_3$H–15 NTs and Si(Et)Si-Ar-SO$_3$H–20 NTs, significantly decreased BET surface area and pore volume are observed. For example, the BET surface area and pore volume is 501 m^2 g^{-1} and 0.45 cm^3 g^{-1} for the Si(Et)Si-Ar-SO$_3$H–20 NTs. The result indicates that most of −Ar-SO$_3$H groups were confined inside the tubes since one-dimensional tubular Si(Et)Si-Ar-SO$_3$H NTs catalysts possess large fraction of voids in the interior. Therefore, incorporation of a large amount of −Ar-SO$_3$H groups could block the tubular channel of the nanohybrids severely, which in turn lead to the decreased BET surface area, pore diameter and pore volume. It should be noted that introduction of suitable amount of arenesulfonic acid group (e.g. lower than 10 mol%) did not influence the porosity of the alkyl-bridged organosilica
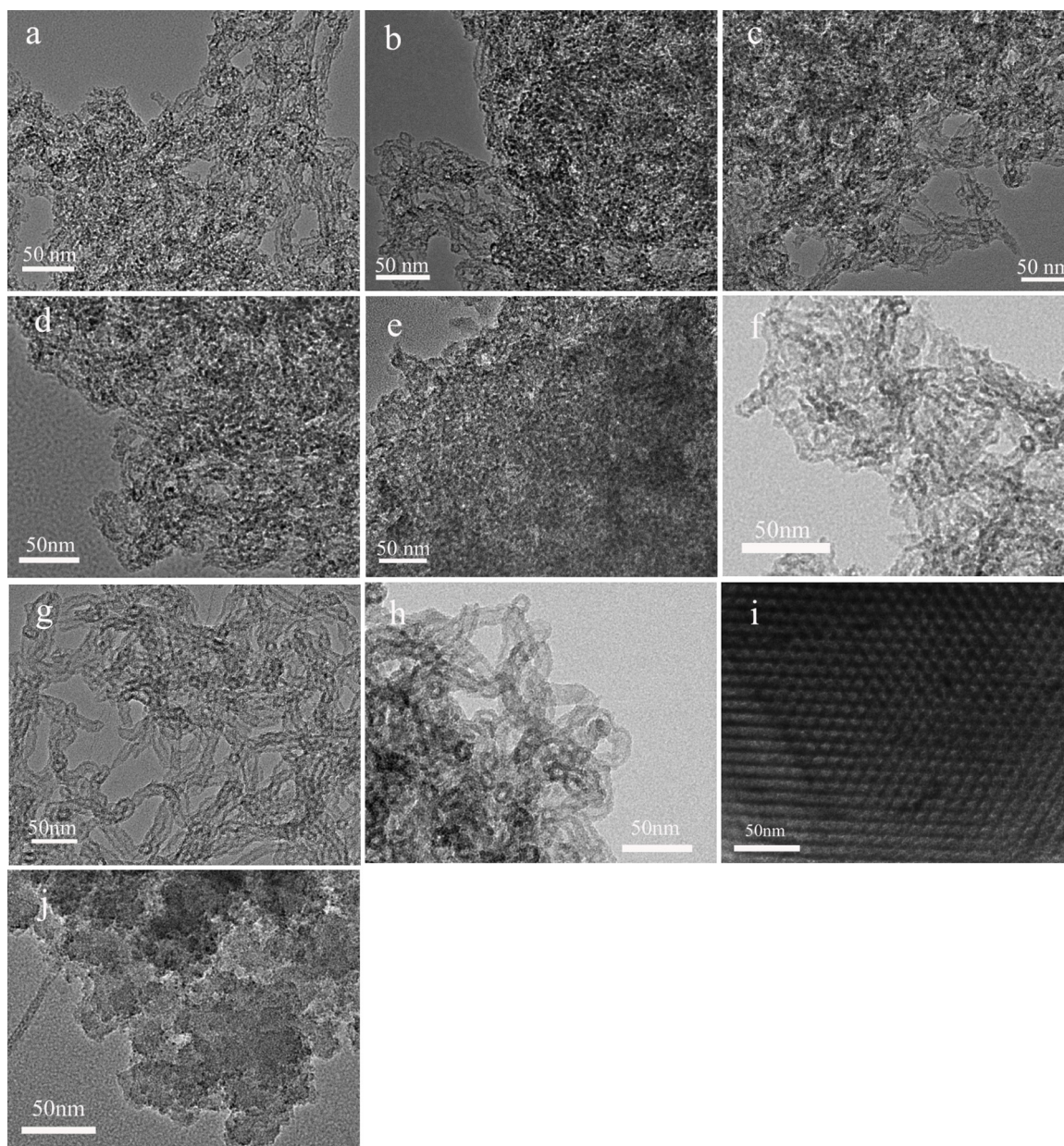
Fig. 1. TEM images of various SO₃H-based hybrid catalysts: (a) Si(Et)Si NTs; (b) Si(Et)Si-Ar-SO₃H–5 NTs; (c) Si(Et)Si-Ar-SO₃H–10 NTs; (d) Si(Et)Si-Ar-SO₃H–15 NTs; (e) Si(Et)Si-Ar-SO₃H–20 NTs; (f) Si(Et)Si-Pr-SO₃H–10 NTs; (g) Si(Ph)Si NTs; (h) Si(Ph)Si-Ar-SO₃H–10 NTs; (i) SBA-15-Ar-SO₃H–10; and (j) P123 free Si(Ph)Si-Ar-SO₃H–10.

Table 1
Textural parameters, acid capacity and sulfur content of various SO₃H-based hybrid catalysts.

Catalysts	S_{BET} [m² g⁻¹][a]	D_p [nm][b]	V_p [cm³ g⁻¹][c]	Acid-site density [μeq(H⁺) g⁻¹][d]	Acid-site density [μeq(SO₃H) g⁻¹][e]
Si(Et)Si NTs	838	5.1/31.7	1.73	–	–
Si(Et)Si-Ar-SO₃H–5 NTs	826	5.0/30.3	1.39	418	509
Si(Et)Si-Ar-SO₃H–10 NTs	833	4.9/22.6	1.63	950	1072
Si(Et)Si-Ar-SO₃H–15 NTs	712	4.8/32.1	1.66	1160	1278
Si(Et)Si-Ar-SO₃H–20 NTs	501	3.8	0.45	1360	1432
Si(Ph)Si NTs	841	4.5/54.2	1.02	–	–
Si(Ph)Si-Ar-SO₃H–10 NTs	804	4.9/23.7	1.65	898	903
Si(Et)Si-Pr-SO₃H–10 NTs	785	4.7/29.9	1.49	930	1090
SBA-15-Ar-SO₃H–10	685	6.5	0.77	922	989
P123 free Si(Ph)Si-Ar-SO₃H–10	430	3.8/48.5	0.39	762	980

[a] Surface area (S_{BET}) was calculated using the Brunauer–Emmett–Teller (BET) equation.
[b] Pore diameter (D_p) was estimated from BJH desorption determination.
[c] Pore volume (V_p) was estimated from the pore volume determination using the adsorption branch of the N₂ isotherm curve at $P/P_0 = 0.99$ single point.
[d] From titration with NaOH (0.0095 mol L⁻¹).
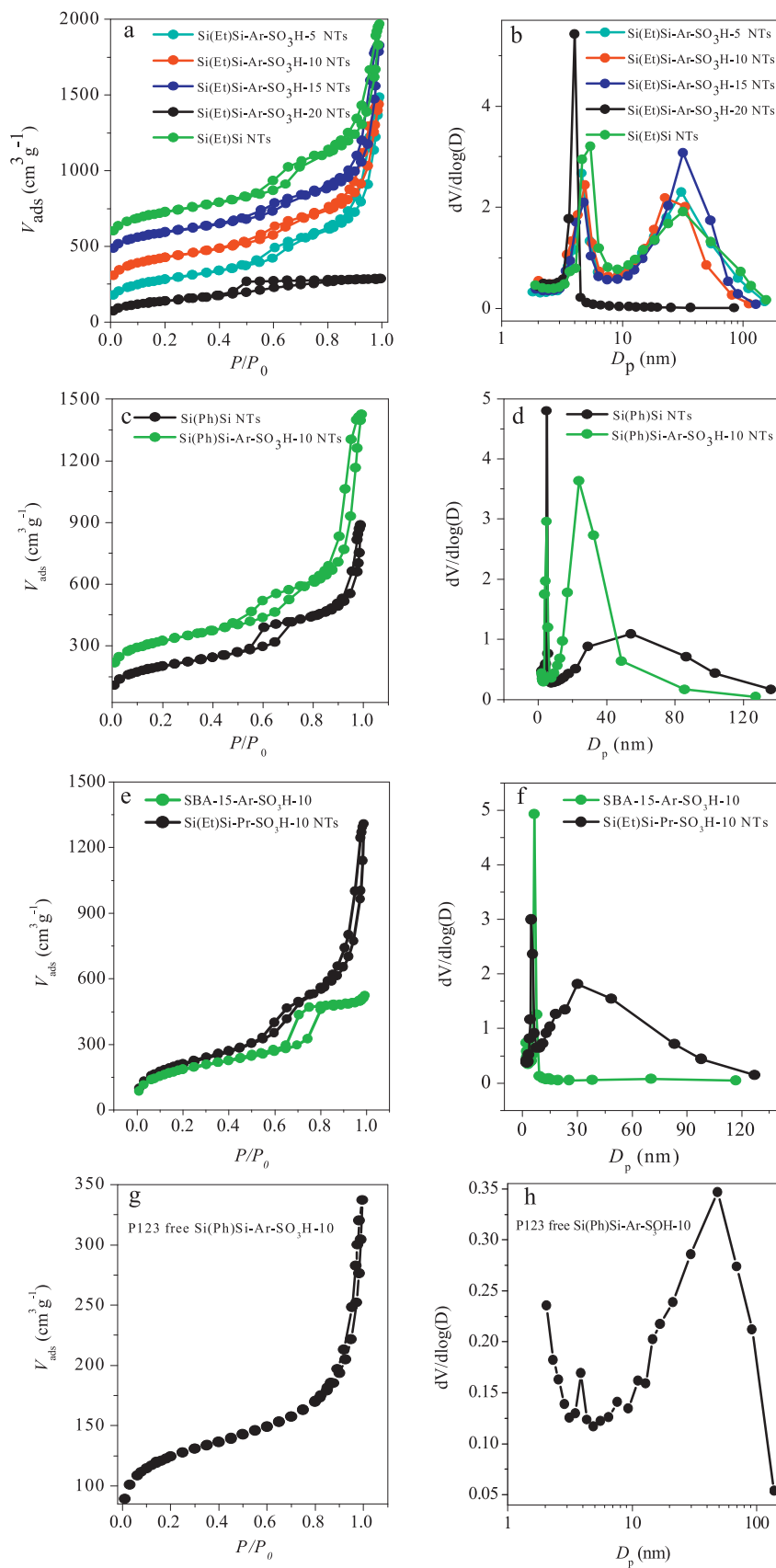[e] From ICP-OES determination.

Fig. 2. Nitrogen gas adsorption–desorption isotherms (a, c, e, g) and BJH pore size distribution profiles (b, d, f, h) of various SO$_3$H-based hybrid catalysts.

nanotubes significantly, and they still exhibit excellent textural properties that are favorable to the catalytic reactions. Additionally, the —Ar/Pr-SO$_3$H-site-confined hollow interiors of the tubular nanohybrids can provide a nanoreactor for esterification or transesterification, ensuring efficient reactant diffusion and acid site accessibility during the reaction. As shown in Fig. 2c–f, arenesulfonic acid functionalized benzene-bridged organosilica nanotubes (Si(Ph)Si-Ar-SO$_3$H–10 NTs) and propylsulfonic acid functionalized ethane-bridged organosilica nanotubes (Si(Et)Si-Pr-SO$_3$H–10 NTs) show the same type of nitrogen gas sorption isotherms and BJH pore-size distribution curves, further confirming the tubular structure of the nanohybrids with excellent textural properties (Table 1). From Fig. 2f it is also found that the secondary pores of Si(Et)Si-Pr-SO$_3$H–10 NTs become more uniform with respect to pure Si(Et)Si NTs, which may be due to the fact that more uniform void space between the Si(Et)Si-Pr-SO$_3$H–10 NTs particles are created after functionalization.

As for the SBA-15-Ar-SO$_3$H-10, it exhibits type IV isotherm with H1 hysteresis loop, signifying the material possess well-ordered *p*6 mm pore structure (centering at 6.5 nm) (Fig. 2e and f). In the case of the P123 free Si(Ph)Si-Ar-SO$_3$H–10 material, it exhibits irregular nitrogen gas sorption isotherm profile and bimodal pore structure (Fig. 2g and h), originating from finer intraggregated pore (3.8 nm) and larger interaggregated pore (48.5 nm). The BET surface area (430 m^2 g^{-1}) and pore volume (0.39 cm^3 g^{-1}) of P123 free Si(Ph)Si-Ar-SO$_3$H-10 sample are the lowest among all tested organosulfonic acid functionalized silica or organosilica materials.

3.1.2. Composition and structural information

Loading of organosulfonic acid group in various as-prepared SO$_3$H-based hybrid catalysts was determined by an ICP-OES after the samples were digested with dilute NaOH solution, and the results are summarized in Table 1. As expected, the determined values are closed to the calculated values.

Structural integrity of silica/carbon (alkyl-bridged organosilica) framework and the incorporated organosulfonic acid group in as-prepared sulfonic acid functionalized organosilica nanotubes were confirmed by ^{29}Si MAS NMR and ^{13}C CP-MAS NMR, and Si(Et)Si-Ar-SO$_3$H–10 NTs and Si(Ph)Si-Ar-SO$_3$H – 10 NTs were selected as the representative samples. Fig. 3 displays ^{29}Si MAS NMR spectrum of both of the nanohybrids, and the characteristic resonances between −58.0 and −80.0 ppm of an organosiloxane network [$T^n = R - Si(OSi)_n(OH)_{3-n}$, $n = 1 - 3$, $R = -CH_2CH_2-$ or $-C_6H_4-$] from BTMSE or BTESB are found. For the Si(Et)Si-Ar-SO$_3$H–10 NTs, it exhibits predominantly signals at −58.8 and −65.9 ppm, corresponding to the siloxane species of $-CH_2CH_2-Si(OSi)_2(OH)$ (T^2) and $-CH_2CH_2-Si(OSi)_3$ (T^3) within the ethane-bridged organosilica groups, respectively (Fig. 3a). In the case of Si(Ph)Si-Ar-SO$_3$H − 10 NTs, three distinct resonance signals at −63.6, −71.9 and −80.0 ppm were detected (Fig. 3b), corresponding to the siloxane species of $-C_6H_4-Si(OSi)(OH)_2$ (T^1), $-C_6H_4-Si(OSi)_2(OH)$ (T^2) and $-C_6H_4-Si(OSi)_3$ (T^3) within the benzene-bridged organosilica groups, respectively [38,39].

^{13}C CP-MAS NMR experiments were subsequently run to check the structural integrity of the ethane- or benzene-bridged moieties and the incorporated arenesulfonic acid group (Fig. 4). Fig. 4a presents ^{13}C CP-MAS NMR spectrum of Si(Et)Si-Ar-SO$_3$H–10 NTs. Five types of carbon species, C^1–C^5, are assigned to arenesulfonic acid groups of the sample: the resonance signals at 16.3 and 29.0 ppm originate from the methylene carbon species (C^1 and C^2 in Fig. 4a) [40], while the peaks at 126.6, 140.6 and 148.1 ppm are assigned to aromatic carbon species (C^3, C^4 and C^5 in Fig. 4a). As for the carbon atoms of bridging ethyl group in the silica/carbon framework, its resonance signal positions at 5.3 ppm (C^6 in Fig. 4a), and it is the most intense peak among all peaks since it comes from BTMSE precursor [24]. Similarly, Si(Ph)Si-Ar-SO$_3$H–10 NTs also possess five
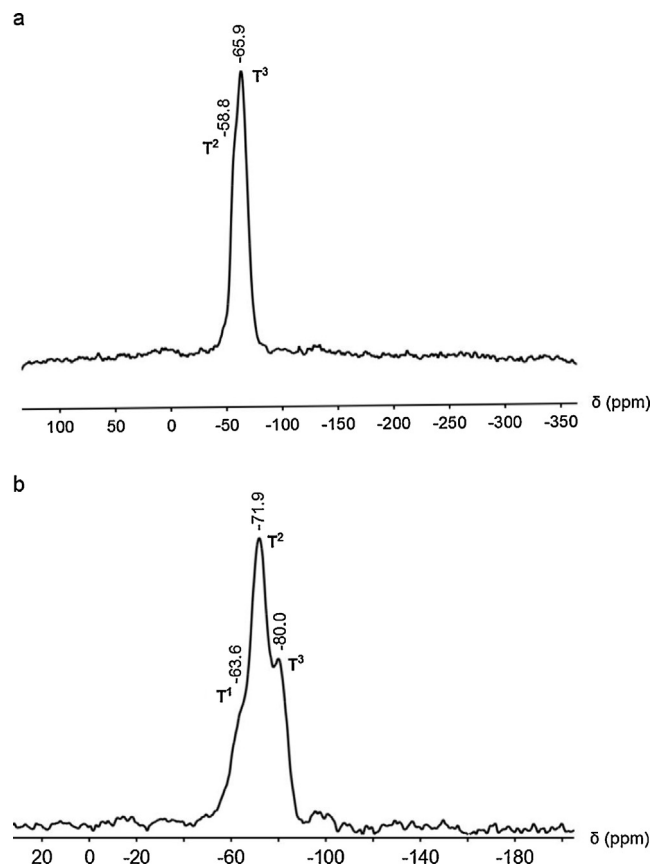
Fig. 3. ^{29}Si MAS NMR spectra of the representative SO$_3$H-based hybrid catalysts: (a) Si(Et)Si-Ar-SO$_3$H–10 NTs, and (b) Si(Ph)Si-Ar-SO$_3$H–10 NTs.

types of carbon species that are related to arenesulfonic acid groups, and these signals positions at 16.2, 28.3, 127.7, 140.3 and 148.2 ppm (C^1–C^5 in Fig. 4b), respectively. In the case of the most intense peak positioned at 133.8 ppm, it corresponds to carbon atoms of bridging phenyl group in organosilica framework (C^6 in Fig. 4b) [41].

The above solid state NMR results demonstrate that organosulfonic acid groups are incorporated to the prepared nanohybrids by current sol–gel co-condensation approach; meanwhile, the absence of any resonance signals assignable to inorganic SiO$_4$ species such as Q^3 [Si(OSi)$_3$(OH), −90 ppm] and Q^4 [Si(OSi)$_4$, −120 ppm] confirms that cleavage of the Si−C bond of Si−R−Si (R = −CH$_2$CH$_2$−/−C$_6$H$_4$−) moiety in the silica/carbon framework has been avoided. Therefore, the wall of arenesulfonic acid functionalized alkyl-bridged organosilica nanotubes is composed of covalently bonded organic-inorganic networks of O$_{1.5}$Si−R−Si−O$_{1.5}$Si−CH$_2$−CH$_2$−C$_6$H$_4$−SO$_3$H, in which alkyl-bridged O$_{1.5}$Si−R−Si−O$_{1.5}$Si moiety originates from bridging organosilane (e.g. BTMSE or BTESB) and CH$_2$−CH$_2$−C$_6$H$_4$−SO$_3$H unit comes from arenesulfonic acid-based precursor (i.e. CSPTMS).

3.1.3. Brønsted acidity

The Brønsted acidity of as-prepared hybrid catalysts is characterized by the acid-site density that is determined by titration with dilute NaOH (0.0095 mol L^{-1}), and the results are listed in the Table 1. For arenesulfonic acid functionalized ethane-bridged organosilica nanotubes, their acid-site density increases gradually with sulfonic acid group loading, i.e., the acid-site density of Si(Et)Si-Ar-SO$_3$H–5 NTs, Si(Et)Si-Ar-SO$_3$H–10 NTs, Si(Et)Si-Ar-SO$_3$H–15 NTs and Si(Et)Si-Ar-SO$_3$H–20 NTs is 418, 950, 1160 and 1360 μeq(H$^+$) g^{-1}, respectively. At the same sulfonic acid group loading (10 mol%) but different bridging alkyl groups (e.g. ethyl

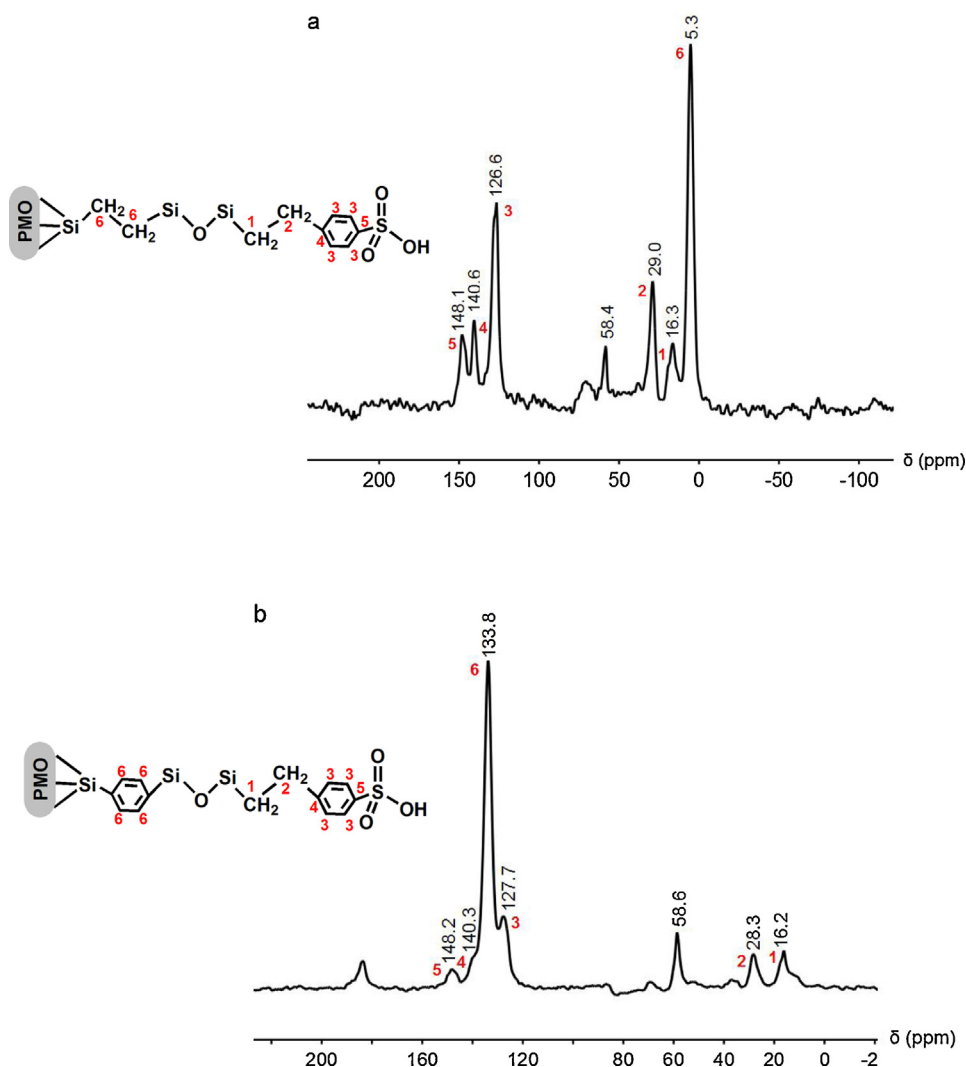**Fig. 4.** ^{13}C CP MAS NMR spectra of the representative SO$_3$H-based hybrid catalysts: (a) Si(Et)Si-Ar-SO$_3$H–10 NTs, and (b) Si(Ph)Si-Ar-SO$_3$H–10 NTs.

or phenyl) or sulfonic acid groups (e.g. arenesulfonic or propyl-sulfonic acid) or silica supports (e.g. organic or inorganic silica), Si(Et)Si-Ar-SO$_3$H–10 NTs (950 μeq(H$^+$) g^{-1}), Si(Ph)Si-Ar-SO$_3$H–10 NTs (898 μeq(H$^+$) g^{-1}), Si(Et)Si-Pr-SO$_3$H–10 NTs (930 μeq(H$^+$) g^{-1}) or SBA-15-Ar-SO$_3$H–10 (922 μeq(H$^+$) g^{-1}), they exhibit the similar acid-site density. In the case of P123 free Si(Ph)Si-Ar-SO$_3$H–10 (762 μeq(H$^+$) g^{-1}), its acid-site density is lower. This is due to the fact that the decreased BET surface area results in minor dispersion of active sites throughout the catalysts. Additionally, the determined acid-site density by ICP-OES method is higher than that of the titration method, suggesting that the real acid-site density is also dominated by the BET surface area of the hybrid catalyst.

3.1.4. Thermal properties

The thermal stability of as-prepared Si(Ph/Et)Si-Ar/Pr-SO$_3$H NTs hybrids is studied by TGA in the range of 25 to 600 °C, and the TGA plots of the representative samples (Si(Et)Si-Ar-SO$_3$H–10 NTs and Si(Ph)Si-Ar-SO$_3$H–10 NTs) are depicted in Fig. 5. The TGA profile shows two weight loss steps: the first weight loss (ca. 10% for Si(Et)Si-Ar-SO$_3$H–10 NTs and 25% for Si(Ph)Si-Ar-SO$_3$H–10 NTs) occurred below 100 °C is related to the loss of physisorbed water at the hybrid material surface. The second weight loss (19.8% for Si(Et)Si-Ar-SO$_3$H–10 NTs and 17.0% for Si(Ph)Si-Ar-SO$_3$H–10 NTs) happened at the temperature higher than 400 °C is attributed to the

decomposition of organic groups in the hybrid materials including bridging ethane or benzene groups and Ar—SO$_3$H groups. Therefore, it is concluded that as-prepared Si(Et/Ph)Si-Pr/Ar-SO$_3$H NTs hybrid materials are thermally stable below 400 °C.

3.2. Evaluation of the heterogeneous acid catalytic activity of organosulfonic acid functionalized alkyl-bridged organosilica nanotubes

3.2.1. Esterification of palmitic acid

The heterogeneous acid catalytic activity of organsulfonic acid functionalized alkyl-bridged organosilica nanotubes was firstly evaluated by esterification of palmitic acid (PA) with methanol to yield methyl palmitate (MP) under the conditions of molar ratio of PA to methanol of 1:5, 2 wt% catalyst, 65 °C and atmospheric pressure (Scheme 2a). The esterification activity of the tested catalysts was represented by the yield of MP.

At first, the catalytic activity of Si(Et)Si-Ar-SO$_3$H NTs hybrid catalysts with various —Ar-SO$_3$H group loadings (e.g. 5, 10, 15 and 20 mol%) in PA esterification were studied to find the optimum sulfonic acid group loading of the tested hybrid catalysts. From the result shown in Fig. 6 it is found that increasing —Ar-SO$_3$H group loading from 5 to 10 mol%, the yield of MP increased, and further increasing the —Ar-SO$_3$H group loading to 15 and 20 mol%, the yield
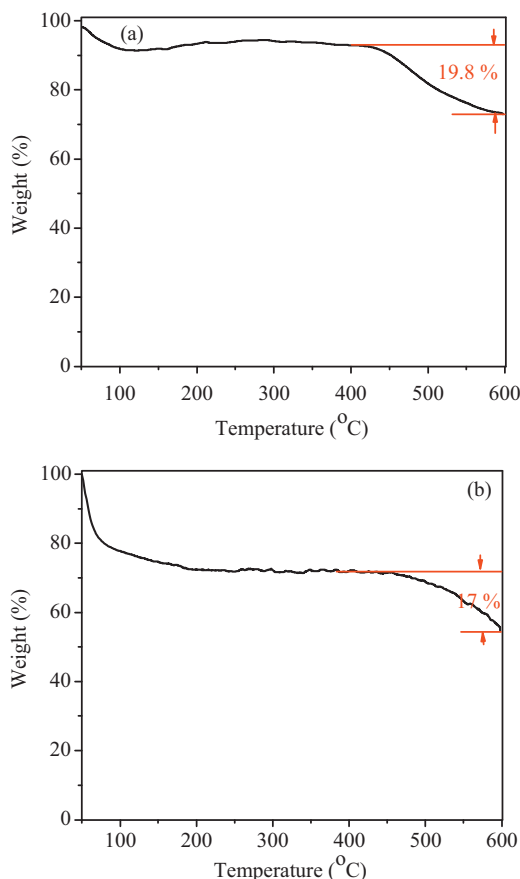
Fig. 5. TDA plots of (a) Si(Et)Si-Ar-SO$_3$H–10 NTs, and (b) Si(Ph)Si-Ar-SO$_3$H–10 NTs.

of MP decreases gradually. For example, after the reaction proceeds for 3 h, the yield of MP is 66.0, 99.9, 87.0, and 81.0%, respectively, for the Si(Et)Si-Ar-SO$_3$H–5 NTs-, Si(Et)Si-Ar-SO$_3$H–10 NTs-, Si(Et)Si-Ar-SO$_3$H–15 NTs- and Si(Et)Si-Ar-SO$_3$H–20 NTs-catalyzed PA esterification reaction. The activity difference among the above four tested hybrid catalysts is explained in terms of their different Brønsted acid-site density, porosity (including BET surface area, pore diameter and pore volume) as well as morphological characteristic. For the Si(Et)Si-Ar-SO$_3$H–5 NTs hybrid catalyst, it has perfect porosity characteristic and tubular microstructure but the lowest Brønsted acid-site density among four test Si(Et)Si-Ar-SO$_3$H NTs hybrid catalysts (Table 1), corresponding to its lowest esterification catalytic activity. In the case of Si(Et)Si-Ar-SO$_3$H–10
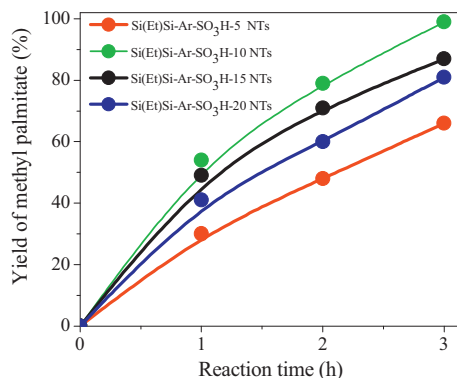

Fig. 6. Catalytic activity of Si(Et)Si-Ar-SO$_3$H NTs hybrid catalysts with various −SO$_3$H group loadings towards esterification of palmitic acid with methanol. Molar ratio of palmitic acid: methanol = 1: 5; 2 wt% catalyst; 65 °C; atmospheric pressure.

NTs, it still possess excellent porosity characteristic and tubular microstructure; meanwhile, its Brønsted acid-site density significantly increases compared with Si(Et)Si-Ar-SO$_3$H–5 NTs, and therefore, it exhibits the highest esterification catalytic activity among all tested hybrid catalysts. The lower esterification catalytic activity of the Si(Et)Si-Ar-SO$_3$H–15 NTs and Si(Et)Si-Ar-SO$_3$H–20 NTs compared with Si(Et)Si-Ar-SO$_3$H–10 NTs is attributed to the obviously decreased BET surface area, pore diameter and pore volume together with obvious aggregation of the tubualr nanoparticles, although they have much higher Brønsted acid-site density. Therefore, it is concluded that the highest esterification catalytic activity of Si(Et)Si-Ar-SO$_3$H–10 NTs hybrid catalyst is due to the combination of large amount of well-distributed −Ar-SO$_3$H sites, perfect porosity and well-defined tubular microstructure. Among these factors, Brønsted acid-site density of the hybrid catalyst plays the paramount role to the esterification catalytic activity based on the Si(Et/Ph)Si-Ar/Pr-SO$_3$H NTs-catalyzed esterification process. At first, the protonation of the carbonyl group of palmitic acid by the Brønsted −SO$_3$H acid sites forms a carbocation of palmitic acid, which is the rate-determining step of the esterification reaction. Secondly, the nucleophilic attack of methanol to the carbocation of palmitic acid produces a tetrahedral intermediate. Finally, the proton migration and breakdown of the intermediate occurs, leading to forming methyl palmitate and water.

On the other hand, morphology and porosity of the hybrid catalysts influence their catalytic activity obviously. One-dimensional tubular Si(Et)Si-Ar-SO$_3$H NTs catalysts possess large fraction of voids in the interior, allowing most of −Ar-SO$_3$H groups being confined inside the tubes. Therefore, −Ar-SO$_3$H-site-confined hollow interiors of the tubular nanohybyid can provide a nanoreactor for esterification reaction, ensuring efficient reactant diffusion and acid site accessibility during the reaction. Additionally, the Si(Et)Si-Ar-SO$_3$H NTs catalysts possess bimodal porous structure with both smaller and larger pore, which also can facilitate mass transport of bulky PA reactant and MP product. Meanwhile, much larger surface area and higher pore volume of the hybrid catalyst can provide higher population of the accessible acid sites. All of these advantages ensure the esterification proceeding at a fast rate.

For the following tests, various sulfonic acid-based catalysts with sulfonic acid group loading of 10 mol% was selected as the representative catalysts.

Secondly, at sulfonic acid group loading of 10 mol%, catalytic activity of various SO$_3$H-based hybrid catalysts including Si(Ph)Si-Ar-SO$_3$H–10 NTs, Si(Et)Si-Ar-SO$_3$H–10 NTs, Si(Et)Si-Pr-SO$_3$H–10 NTs and SBA-15-Ar-SO$_3$H–10 towards PA esterification reaction was tested to find out the influence of types of bridging alkyl group (which is selected to adjust the surface hydrophobicity and porosity of the catalyst), types of −SO$_3$H groups (which is selected to adjust the Brønsted acid strength of the catalyst) and morphology on the esterification activity. For comparison, commercial available Amberlyst-15, a macroporous sulfonic acid ion-exchange resin that is widely used in biodiesel production, was also tested under the same conditions. From the result shown in Fig. 7 it is found that five SO$_3$H-based catalysts follow the activity order Si(Ph)Si-Ar-SO$_3$H–10 NTs > Si(Et)Si-Ar-SO$_3$H–10 NTs > Si(Et)Si-Pr-SO$_3$H–10 NTs > SBA-15-Ar-SO$_3$H–10 > Amberlyst-15. For example, for the Si(Ph)Si-Ar-SO$_3$H–10 NTs-, Si(Et)Si-Ar-SO$_3$H–10 NTs-, Si(Et)Si-Pr-SO$_3$H–10 NTs-, SBA-15-Ar-SO$_3$H–10- and Amberlyst-15-catalyzed PA esterification reaction, the yield of MP reaches 87.3, 78.8, 75.4, 66.7 and 33.8%, respectively, over period of 2 h. Further increasing the reaction time to 3 h, the yield of MP reaches to 100% for the Si(Ph)Si-Ar-SO$_3$H–10 NTs- or Si(Et)Si-Ar-SO$_3$H–10 NTs-catalyzed esterification reaction. Amberlyst-15 is one of the efficient esterification catalysts with very high acid-site density ($4800\ \mu eq(H^+)\,g^{-1}$), however, four as-prepared SO$_3$H-based hybrid catalysts show obviously higher PA esterification activity than that
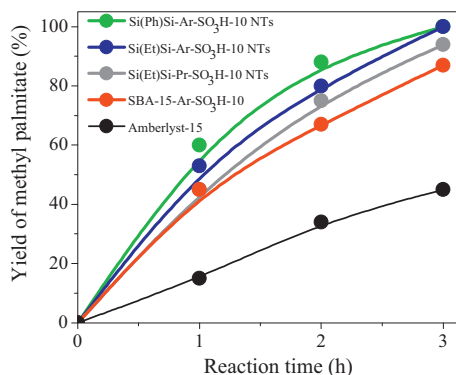
Fig. 7. Catalytic activity of various SO_3H-based hybrid catalysts towards esterification of palmitic acid with methanol. For comparison, Amberlyst-15 was also tested. Molar ratio of palmitic acid: methanol = 1: 5; 2 wt% catalyst; 65 °C; atmospheric pressure.

of Amberlyst-15. The lower activity of Amberlyst-15 is due to its smaller surface area, which leads to poor accessibility of the acid sites to the reactants. The excellent catalytic activity of as-prepared hybrid catalysts is explained in terms of hydrophobicity, tube-like morphology, and Brønsted acid strength.

On the one hand, the enhanced surface hydrophobicity owing to the introduction of bridging alkyl groups gives the positive influence on the PA esterification activity. Water is the byproduct of esterification reaction, and it favors to adsorb on the surface of hydrophilic catalysts (*e.g.* sulfonic acid-based silica catalyst), which prevent hydrophobic PA molecule from the adsorption on the catalyst surface; additionally, esterification is a reversible process, and the produced ester molecules can easily be hydrolyzed by water. Both of factors result in the decreased MP formation rate [17]. The problems can be alleviated by functionalization of sulfonic acid-based silica materials with hydrophobic alkyl groups, which can selectively create an unsuitable environment for water molecule and lead to them easy escape from the catalyst surface. Consequently, the accessibility of the acid sites to the hydrophobic PA may be increased and thereby accelerating the reaction rate; meanwhile, deactivation of the acid sites owing to the strong adsorption of water molecules on the catalyst surface is inhibited. Therefore, Si(Ph)Si-Ar-SO$_3$H–10 NTs or Si(Et)Si-Ar-SO$_3$H–10 NTs with bridging phenyl or ethyl groups in the silica network show considerably higher activity towards the target esterification reaction compared with alkyl-free SBA-15-Ar-SO$_3$H–10. As for the Si(Ph)Si-Ar-SO$_3$H–10 NTs and Si(Et)Si-Ar-SO$_3$H–10 NTs, higher catalytic activity of the former than the latter is owing to more hydrophobic characteristic of phenyl group than that of ethyl group. Additionally, it should be noted that the inner diameter of the Si(Ph)Si-Ar-SO$_3$H–10 NTs (ca. 9 nm) is larger than that of the Si(Et)Si-Ar-SO$_3$H–10 NTs (ca. 7 nm). The larger inner diameter is more favorable to accommodate large PA molecules, giving a positive influence on the esterification activity of the Si(Ph)Si-Ar-SO$_3$H–10 NTs.

On the other hand, compared with two-dimensional hexagonal mesoporous SBA-15-Ar-SO$_3$H–10 catalyst, one-dimensional tubular sulfonic acids functionalized alkyl-bridged organosilica nanotubes catalysts possess much larger BET surface area and higher pore volume. Meanwhile, they possess large fraction of voids in the interior, allowing most of the active sites being confined inside the tubes except for external surface. Additionally, the hierarchical pore systems originate from hollow nanotube channels and void space between tubular nanoparticles are highly accessible to bulky palmitic acid molecules and favorable to efficient reactant diffusion during the catalytic reactions. These advantageous ensure

the tubular Si(Et/Ph)Si-Ar-SO$_3$H NTs superior catalytic activity to the mesostructured SBA-15-Ar-SO$_3$H–10.

In the cases of arenesulfonic and propylsulfonic acid functionalized ethyl-bridged organosilica nanotubes catalysts, Si(Et)Si-Ar-SO$_3$H–10 NTs and Si(Et)Si-Pr-SO$_3$H–10 NTs, they possess similar textural properties and acid-site density but different catalytic activity. This is due to their different acid strength that is mainly determined by the microenvironment of the SO$_3$H sites in both catalysts [11,36]. For Si(Et)Si-Ar-SO$_3$H–10 NTs catalyst, phenyl in the arenesulfonic acid group can provide stronger electron withdrawing environments than propyl in propylsulfonic acid group of Si(Et)Si-Pr-SO$_3$H–10 NTs catalyst, leading to Si(Et)Si-Ar-SO$_3$H–10 NTs higher Brønsted acid strength and thereby higher catalytic activity in the target reaction than that of Si(Et)Si-Pr-SO$_3$H–10 NTs.

Combination of the results displayed in Figs. 6 and 7 it is inferred that Brønsted acid strength and acid-site density play a dominated role to the excellent esterification activity of as-prepared organosulfonic acid functionalized alkyl-bridged organosilica nanotubes hybrid catalysts; additionally, the catalytic activity is also determined to a great extent by their enhanced surface hydrophobicity, excellent porosity properties and interesting tube-like morphology.

3.2.2. Transesterification of yellow horn seed oil

The heterogeneous acid catalytic activity of organosulfonic acid functionalized alkyl-bridged organosilica nanotubes was further tested by transesterification of yellow horn seed oil under refluxing temperature (65 °C) and atmospheric pressure (Scheme 2b), and Si(Ph)Si-Ar-SO$_3$H–10 NTs and Si(Et)Si-Ar-SO$_3$H–10 NTs were selected as the representative catalysts. Unlike one step esterification reaction, transesterification is multistep reaction with many intermediates, and therefore, it proceeds at a significantly slower reaction rate, especially under mild conditions rather than at higher temperature and higher pressure.

Yellow horn is an ideal energy crop, which can be widely planted against drought, cold, salt and starvation because of the advantages associated with its high oil content (55–65%). Moreover, yellow horn seed oil is of high unsaturated triglycerides (TGs) content (85–93%) and low acid value (0.5–0.7 mg KOH/g), so that it can be used as high-quality feedstock for biodiesel production [42]. Based on the literature results and current GC-MS analysis, six FAME products were identified in the Si(Ph/Et)Si-Ar-SO$_3$H–10 NTs-catalyzed yellow horn seed oil transesterification reaction, and they are methyl palmitate (MP), methyl stearate (MS), methyl oleate (MO) and methyl lioleate (ML) together with a small quantity of methyl eicosenoate (ME) and methyl docosanoate (MD). The transesterification activity of the Si(Ph/Et)Si-Ar-SO$_3$H–10 NTs is represented by the yields of four main products including MP, MS, MO and ML.

Fig. 8 displays the kinetic studies of Si(Ph)Si-Ar-SO$_3$H–10 NTs- and Si(Et)Si-Ar-SO$_3$H–10 NTs-catalyzed yellow horn seed oil transesterification reaction. It shows that Si(Ph)Si-Ar-SO$_3$H–10 NTs exhibits higher catalytic activity than that of Si(Et)Si-Ar-SO$_3$H–10 NTs, consistent with their esterification activity. Additionally, in current catalytic systems, the yields of MP, MS, MO and ML are very similar. That is, for the Si(Ph)Si-Ar-SO$_3$H–10 NTs-catalyzed yellow horn seed oil transesterification reaction, the yields of MP, MS, MO and ML are 75.1, 81.5, 79.9 and 73.2%, respectively, after the reaction proceeded for 24 h; under the same conditions, the yields of MP, MS, MO and ML reach 60.6, 65.5, 64.3 and 60.2%, respectively, for the Si(Et)Si-Ar-SO$_3$H–10 NTs-catalyzed transesterification reaction.

Subsequently, at the same sulfonic acid group loading (10 mol%), the catalytic activity of various SO$_3$H-based hybrid catalysts in transesterification reaction were further compared, and Amberlyst-15 was selected as the reference catalyst. From the results presented in Fig. 9 it can be seen that the tested catalysts
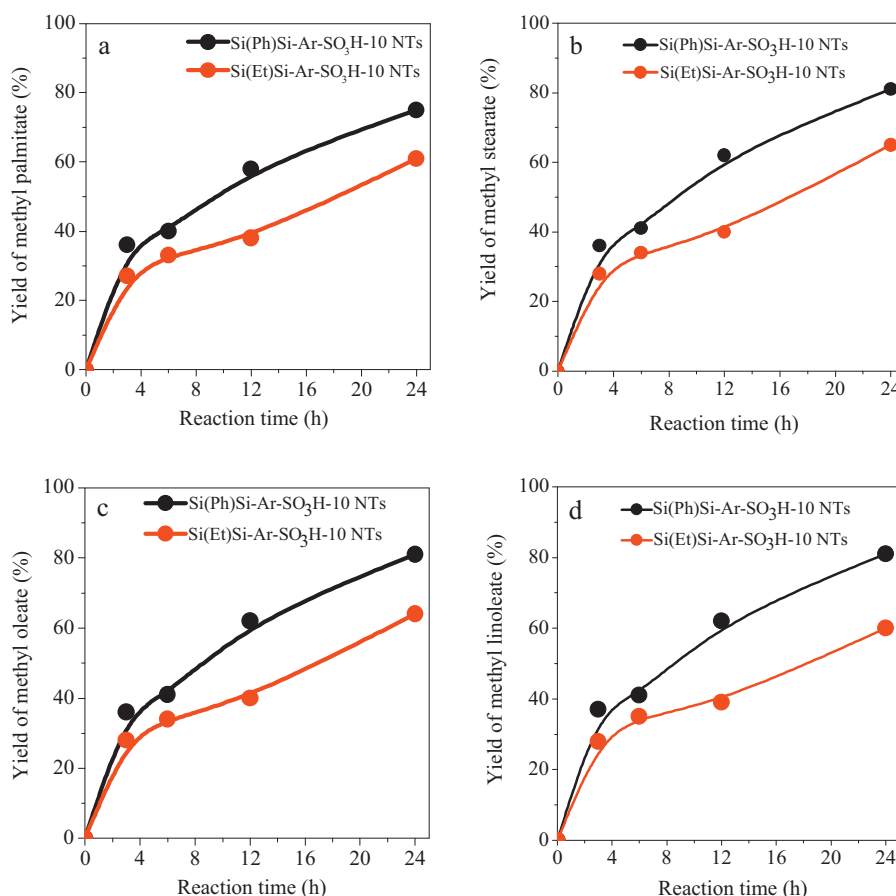
Fig. 8. Catalytic activity of the representative SO$_3$H-based hybrid catalysts, Si(Et)Si-Ar-SO$_3$H–10 NTs and Si(Ph)Si-Ar-SO$_3$H–10 NTs, towards transesterification of yellow horn seed oil with methanol. Oil 1.1 mmol; methanol 3.84 mL; catalyst 5 wt%; 65 °C; 24 h; atmospheric pressure.

follow the activity order Si(Ph)Si-Ar-SO$_3$H–10 NTs > Si(Et)Si-Ar-SO$_3$H–10 NTs > P123 free Si(Ph)Si-Ar-SO$_3$H–10 > Si(Et)Si-Pr-SO$_3$H–10 NTs > SBA-15-Ar-SO$_3$H–10 > Amberlyst-15. The result is similar to that of the above PA esterification tests, further confirming that the transesterification activity of as-prepared SO$_3$H-based hybrid catalysts is determined by their Brønsted acid strength and acid-site density as well as surface hydrophobicity, porosity properties and interesting tube-like morphology. For P123 free Si(Ph)Si-Ar-SO$_3$H–10 catalyst, its lower catalytic activity compared with Si(Ph)Si-Ar-SO$_3$H–10 NTs is due to its poor

porosity and disordered interconnected morphology although it has the similar Brønsted acid strength and acid-site density as well as surface hydrophobicity to the latter. Contribution of surface hydrophobicity on the yellow horn seed oil transesterification reaction is explained by the following two aspects. On one hand, surface hydrophobic Si(Ph/Et)Si-Ar/Pr-SO$_3$H hybrid catalysts can selectively create an unsuitable environment for adsorption of hydrophilic byproducts (e.g. water and glycerol), leading to them easy desorption from the catalyst surface; meanwhile, adsorption and diffusion of hydrophobic TG reactants is improved. On the other hand, the acid site deactivation due to the strong adsorption of water or glycerol on the catalyst surface is inhibited. As a consequence, the transesterification reactions can carry out at a faster rate.

3.2.3. Regeneration and reusability

One of the most important factors of heterogeneous catalysts contributing to catalytic performance is the stability against leaching of the active sites during reaction. To evaluate this performance, the most active Si(Ph)Si-Ar-SO$_3$H–10 NTs hybrid catalyst is selected for esterification of PA and transesterification of yellow horn seed oil with methanol. After each catalytic cycle, the catalyst is recovered by centrifugation, and then it is washed with dichloromethane three times. After being dried at 60 °C overnight, the catalyst was weighed and applied to subsequent the 2nd and 3rd cycles under the same conditions. As shown in Figs. 10 and 11, the catalytic activity of Si(Ph)Si-Ar-SO$_3$H–10 NTs for the formation of FAMEs including MP, MS, MO and ML remained constant after it has been reused for three times. The lack of degradation of activity after the third run demonstrates that the sulfonic acid groups are
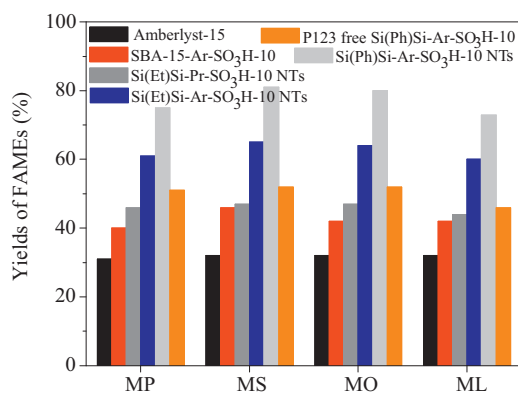

Fig. 9. Catalytic activity of various SO$_3$H-based hybrid catalysts towards transesterification of yellow horn seed oil with methanol. Oil 1.1 mmol; methanol 3.84 mL; catalyst 5 wt%; 65 °C; 24 h; atmospheric pressure.
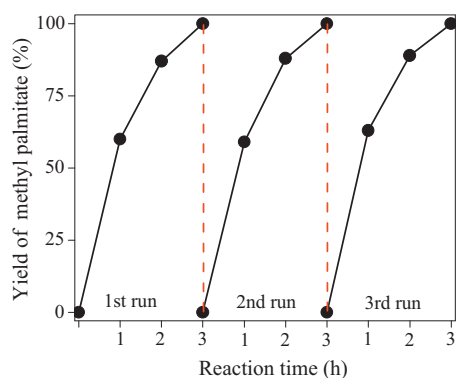
Fig. 10. Recyclability of the representative SO$_3$H-based hybrid catalyst, Si(Ph)Si-Ar-SO$_3$H–10 NTs, towards esterification of palmitic acid with methanol under the conditions of molar ratio of palmitic acid: methanol = 1: 5; 2 wt% catalyst; 65 °C; atmospheric pressure.
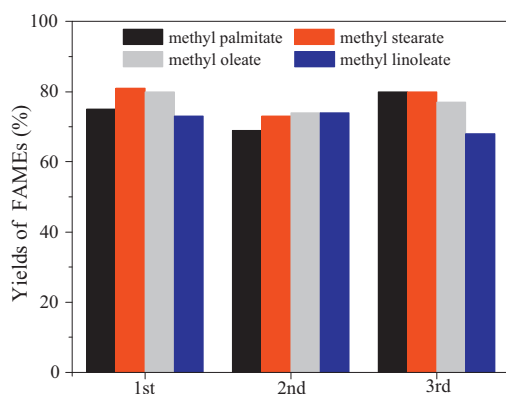

Fig. 11. Recyclability of the representative SO$_3$H-based hybrid catalyst, Si(Ph)Si-SO$_3$H–10 NTs, towards transesterification of yellow horn seed oil with methanol. Oil 1.1 mmol; methanol 3.84 mL; catalyst 5 wt%; 65 °C; 24 h; atmospheric pressure.

strongly bonded to the silica/carbon framework and remain available as acid sites; meanwhile, catalyst deactivation due to the strong adsorption of hydrophilic byproducts is inhibited owing to its surface hydrophobicity. The prepared hybrid catalysts therefore have promising potential for working as the efficient and stable solid acid catalysts in both esterification and transesterification reactions.

4. Conclusions

Arenesulfonic or propylsulfonic acid functionalized ethane- or benzene-bridged organosilica nanotubes hybrid catalysts were successfully prepared by careful designing a single step nonionic surfactant-templated sol–gel co-condensation route. After formation of the nanohybrids, the structural integrity of organosulfonic acid groups and silica/carbon framework remained intact, and the interesting tube-like morphology led to the hybrid catalysts unique porosity characteristic including much larger BET surface area, higher pore volume and bimodal pore structure with both smaller and larger pores. Among the tested Si(Ph/Et)Si-Ar/Pr-SO$_3$H NTs nanohybrids and the reference catalysts (i.e. SBA-15-Ar-SO$_3$H, P123 free Si(Ph)Si-Ar-SO$_3$H and Amberlyst-15), arenesulfonic acid functionalized benzene-bridged organosilica nanotubes with arenesulfonic acid group loading of 10 mol% (i.e. Si(Ph)Si-Ar-SO$_3$H–10 NTs) exhibited the highest catalytic activity in esterification of palmitic acid and transesterification of yellow horn seed oil with methanol under mild conditions, attributed to the combination

of considerably high Brønsted acid strength and acid-site density, enhanced surface hydrophobicity, unique porosity properties and perfect tube-shaped morphology. As-prepared hybrid catalysts can be used at least three times without obvious activity loss, exhibiting potential as the efficient and stable solid acid catalysts in biodiesel production from low cost inedible feedstocks.

References

[1] K. Wilson, A.F. Lee, Catal. Sci. Technol. 2 (2012) 884–897.
[2] Y.B. Huang, Y. Fu, Green Chem. 15 (2013) 1095–1111.
[3] Y.C. Sharma, B. Singh, J. Korstad, Biofuels, Bioprod. Bioref. 5 (2011) 69–92.
[4] J.A. Melero, J. Iglesias, G. Morales, Green Chem. 11 (2009) 1285–1308.
[5] B.M. Reddy, M.K. Patil, Chem. Rev. 109 (2009) 2185–2208.
[6] W. Li, Z.J. Jiang, F.Y. Ma, F. Su, L. Chen, S.Q. Zhang, Y.H. Guo, Green Chem. 12 (2010) 2135–2138.
[7] W. Li, F.Y. Ma, F. Su, L. Ma, S.Q. Zhang, Y.H. Guo, ChemCatChem 4 (2012) 1798–1807.
[8] W. Li, F.Y. Ma, F. Su, L. Ma, S.Q. Zhang, Y.H. Guo, ChemSusChem 4 (2011) 744–756.
[9] A.A. Kiss, A.C. Dimian, G. Rothenberg, Adv. Synth. Catal. 348 (2006) 75–81.
[10] E. Andrijanto, E.A. Dawsona, D.R. Brown, Appl. Catal. B: Environ. 115/116 (2012) 261–268.
[11] D. Zuo, J. Lane, D. Culy, M. Schultz, A. Pullar, M. Waxman, Appl. Catal. B: Environ. 129 (2013) 342–350.
[12] K. Nakajima, M. Hara, ACS Catal. 2 (2012) 1296–1304.
[13] F.H. Cao, Y. Chen, F.Y. Zhai, J. Li, J.H. Wang, X.H. Wang, S.T. Wang, W.M. Zhu, Biotechnol. Bioeng. 101 (2008) 93–100.
[14] K.X. Li, J.L. Hu, W. Li, F.Y. Ma, L.L. Xu, Y.H. Guo, J. Mater. Chem. 19 (2009) 8628–8638.
[15] L.L. Xu, Y.H. Wang, X. Yang, J.L. Hu, W. Li, Y.H. Guo, Green Chem. 11 (2009) 314–317.
[16] L.L. Xu, W. Li, J.L. Hu, X. Yang, Y.H. Guo, Appl. Catal. B: Environ. 90 (2009) 587–594.
[17] F. Su, Q.Y. Wu, D.Y. Song, X.H. Zhang, M. Wang, Y.H. Guo, J. Mater. Chem. A 1 (2013) 13209–13221.
[18] F. Su, L. Ma, D.Y. Song, X.H. Zhang, Y.H. Guo, Green Chem. 15 (2013) 885–890.
[19] F.J. Liu, L. Wang, Q. Sun, L.F. Zhu, X.J. Meng, F.S. Xiao, J. Am. Chem. Soc. 134 (2012) 16948–16950.
[20] E. Serrano, N. Linares, J. Garcia-Martinez, J.R. Berenguer, ChemCatChem 5 (2013) 844–860.
[21] A. Bail, V.C. Santosa, M.R. Freitas, L.P. Ramosb, W.H. Schreiner, G.P. Ricci, K.J. Ciuffi, S. Nakagaki, Appl. Catal. B: Environ. 130–131 (2013) 314–324.
[22] G.M. Ziarani, A.-R. Badiei, M. Azizi, Sci. Iranica 18 (2011) 453–457.
[23] T.M. Suzuki, T. Nakamura, E. Sudo, Y. Akimoto, K. Yano, Micropor. Mesopor. Mater. 111 (2008) 350–358.
[24] M.H. Tucker, A.J. Crisci, B.N. Wigington, N. Phadke, R. Alamillo, J. Zhang, S.L. Scott, J.A. Dumesic, ACS Catal. 2 (2012) 1865–1876.
[25] J.A. Bootsma, B.H. Shanks, Appl. Catal. A: Gen. 327 (2007) 44–51.
[26] J.A. Melero, L.F. Bautista, G. Morales, J. Iglesias, D. Briones, Energy Fuels (23) (2009) 539–547.
[27] J.P. Lourenço, M.I. Macedo, A. Fernandes, Catal. Commun. 19 (2012) 105–109.
[28] S.J. Miao, B.H. Shanks, Appl. Catal. A: Gen. 359 (2009) 113–120.
[29] W. Schmidt, ChemCatChem 1 (2009) 53–67.
[30] L. Torrente-Murciano, A.A. Lapkin, D. Chadwick, J. Mater. Chem. 20 (2010) 6484–6489.
[31] C. Baleizão, B. Gigante, H. Garcia, A. Corma, J. Catal. 221 (2004) 77–84.
[32] F. Clippel, M. Dusselier, S.V. Vyver, L. Peng, P.A. Jacobs, B.F. Sels, Green Chem. 15 (2013) 1398–1430.
[33] X.B. Li, Y. Yang, Q.H. Yang, J. Mater. Chem. A 1 (2013) 1525–1535.
[34] X. Liu, X.B. Li, Z.H. Guan, J. Liu, J. Zhao, Y. Yang, Q.H. Yang, Chem. Commun. 47 (2011) 8073–8075.
[35] F. Hoffmann, M. Cornelius, J. Morell, M. Fröba, Angew. Chem. Int. Ed. 45 (2006) 3216–3251.
[36] K. Nakajima, I. Tomita, M. Hara, S. Hayashi, K. Domen, J.N. Kondo, Adv. Mater. 17 (2005) 1839–1842.
[37] M. Mandal, M. Kruk, Chem. Mater. 24 (2011) 123–132.
[38] S.Y. Chen, C.Y. Huang, T. Yokoi, C.Y. Tang, S.J. Huang, J.J. Lee, J.C.C. Chan, T. Tatsumi, S. Cheng, J. Mater. Chem. 22 (2012) 2233–2243.
[39] M. Karaki, A. Karout, J. Toufaily, F. Rataboul, N. Essayem, B. Lebeau, J. Catal. 305 (2013) 204–216.
[40] J.A. Melero, G.D. Stucky, R. van Grieken, G. Morales, J. Mater. Chem. 12 (2002) 1664–1670.
[41] Y. Goto, S. Inagaki, Chem. Commun. (2002) 2410–2411.
[42] J. Li, Y.G. Zu, Y.J. Fu, Y.C. Yang, S.M. Li, Z.N. Li, W. Michael, Innov. Food Sci. Emerg. Technol. 11 (2010) 637–643.